Geophysical Journal International

*Geophys. J. Int.* (2017) **210,** 184–195
GJI Marine geosciences and applied geophysics

doi: 10.1093/gji/ggx150

# Structure-, stratigraphy- and fault-guided regularization in geophysical inversion

Xinming Wu

*Bureau of Economic Geology, The University of Texas at Austin, Austin, TX, USA. E-mail: xinming.wu@beg.utexas.edu*

Accepted 2017 April 13. Received 2017 March 23; in original form 2016 September 12

## SUMMARY

Geophysical inversion is often ill-posed because of inaccurate and insufficient data. Regularization is often applied to the inversion problem to obtain a stable solution by imposing additional constraints on the model. Common regularization schemes impose isotropic smoothness on solutions and may have difficulties in obtaining geologically reasonable models that are often supposed to be anisotropic and conform to subsurface structural and stratigraphic features. I introduce a general method to incorporate constraints of seismic structural and stratigraphic orientations and fault slips into geophysical inversion problems. I first use a migrated seismic image to estimate structural and stratigraphic orientations and fault slip vectors that correlate fault blocks on opposite sides of a fault. I then use the estimated orientations and fault slips to construct simple and convenient anisotropic regularization operators in inversion problems to spread information along structural and stratigraphic orientations and across faults. In this way, we are able to compute inverted models that conform to seismic reflectors, faults and stratigraphic features such as channels. The regularization is also helpful to integrate well-log properties into the inversion by spreading the measured rock properties away from the well-log positions into the whole inverted model across faults and along structural and stratigraphic orientations. I use a 3-D synthetic example of impedance inversion to illustrate the structure-, stratigraphy- and fault-guided regularization method. I further applied the method to estimate seismic interval velocity and to compute structure- and stratigraphy-oriented semblance.

**Key words:** Image processing; Inverse theory; Joint inversion; Numerical approximations and analysis.

## 1 INTRODUCTION

Geophysical inversion is an important technique to estimate subsurface models from observed geophysical data. Most geophysical inversion problems are ill-posed because of incorrect formulation of the problems (Tikhonov 1963) and inaccurate and insufficient data (Jackson 1972). Regularization, first introduced by Tikhonov (1963) and others, is commonly used to make the inversion problems well-posed and yield stable solutions by imposing additional constraints on the models to be estimated (e.g. Engl *et al.* 1996; Zhdanov 2002; Fomel 2007). The additional constraints often include some priori knowledge or expectations of the inverted models such as flatness or smoothness (VanDecar & Snieder 1994).

Popular methods of imposing smoothness on models include gradient or first derivative regularization (e.g. Inoue *et al.* 1990; Boschi & Dziewonski 1999) and Laplacian or second derivative regularization (e.g. VanDecar & Snieder 1994; Trampert & Woodhouse 1995). By minimizing the gradient or divergence of gradient (Lapacian) of a model, both methods impose isotropic smoothness on the model. However, a subsurface model is rarely isotropic in space, instead it often contains highly anisotropic structures which appear linear in 2-D and planar in 3-D space.

With this observation, some authors (e.g. Li & Oldenburg 2000; Clapp *et al.* 2004; Hale 2013c) use structural dips to construct anisotropic regularization in which directional derivatives of the model are minimized to impose anisotropic smoothness on the model along structural dips. Ma *et al.* (2012) and Zhou *et al.* (2014) incorporate structural constraints into full waveform inversion and electrical resistivity inversion through an image-guided interpolation method (Hale 2010). The structural or dip constraints are helpful for these methods to compute geologically reasonable models that are smooth and continuous along linear or planar subsurface structure features. Such structural constraints are also incorporated into hydraulic tomography (Ahmed *et al.* 2015) and into a stochastic approach for generating prior geological models (Zhou *et al.* 2016).

However, a geophysical model is not necessarily lateral continuous or smooth, for example, near a fault. On the opposite sides of a fault, the model is significantly discontinuous or displaced due to the movement of the hanging wall and footwall blocks of the fault. Therefore, some authors (e.g. Valenciano *et al.* 2004; Zhang & Zhang 2012) propose to use edge-preserving regularization to preserve fault discontinuities in the estimated models by weighting out the smoothness regularization near the fault positions. In this way, the property discontinuity can be preserved at a fault in

the model, however, the property information on opposite sides of the fault is also prevented from spreading across the fault. In order to spread property information across faults, Zhang & Revil (2015) propose a method to account for fault displacements or slips into geophysical inversion. However, the fault slips are assumed to be spatially invariant, which is not necessarily true in practice. For most faults, especially the growing faults (e.g. the growing faults in the Gulf Coast of Mexico around salt structures (Revil & Cathles 2002, e.g.)), the fault slips often vary along a fault surface in both strike and dip directions.

Although seismic structural constraints have been incorporated into geophysical inversion in numerous methods to compute a subsurface model conforming to seismic reflections, seismic stratigraphic features such as channels are still not used to guide the inversion. In 3-D cases, subsurface rock properties should also be spatially consistent with the seismic stratigraphic features. In addition, to preserve discontinuities at faults, most methods simply use pre-computed fault positions to stop smoothness regularization at faults in the inversion problems. These methods, however, are not able to spread information across faults. In addition, most structure-guided inversion methods are dealing with 2-D inversion while 3-D cases are not well discussed. To address these problems, I propose a general method to construct structure-, stratigraphy- and fault-guided regularization for geophysical inversion to obtain inverted models that conform to subsurface structures, stratigraphic features (such as channels), and faults. I also discuss how to use this regularization method to incorporate well-log constraints into geophysical inversion.

In this proposed method, I first use structure tensors (Van Vliet & Verbeek 1995; Weickert 1997; Fehmers & Höcker 2003; Hale 2009b) to estimate orientations of structural and stratigraphic features from a migrated seismic image. The structure tensors are computed as smoothed outer products of image gradients, and the eigenvectors of the tensors provide estimations of seismic structural and stratigraphic orientations. I also estimate fault slip vectors that correlate seismic reflectors on opposite sides of faults using the methods discussed by Wu & Hale (2016) and Wu *et al.* (2016). In these methods, the fault surfaces are first extracted from a seismic image and fault slips are then estimated by correlating seismic reflections on opposite sides of each fault using dynamic image warping (Hale 2013a). The fault slips computed in this way are allowed to be spatially variant (Wu & Hale 2016; Wu *et al.* 2016) in both fault strike and dip directions.

I then use the estimated orientations and fault slips to construct structure-, stratigraphy- and fault-guided regularization for geophysical inversions. The structure- and stratigraphy-guided regularization imposes smoothness on the model and spreads information in the model along structural and stratigraphic features. The regularization smoothness is anisotropic in most areas where the structural and stratigraphic features are linear or planar but is isotropic in areas where the features are isotropic. This means that the anisotropy or isotropy of the regularization is allowed to be spatially variant. The fault-guided regularization can preserve property discontinuities at the faults in the estimated model and spread property information across faults following the fault slips. Such structure-, stratigraphy-, and fault-guided regularization is also helpful to inversion problems with hard constraints from well-log measurements. The well-log constraints can often provide geological reliable references to calibrate subsurface models but are measured only at limited local positions and therefore can provide only local control in the inversion. The regularization is helpful to provide a more global control from the constraints by spreading the measured properties away from the well-log positions into the whole model across faults and along structural and stratigraphic orientations.

## 2 STRUCTURAL AND STRATIGRAPHIC ORIENTATIONS

To incorporate structural and stratigraphic constraints into geophysical inversion problems, we first need to estimate orientations of structural and stratigraphic features from a seismic image. Several methods, such as the structure tensor (Van Vliet & Verbeek 1995; Weickert 1997; Fehmers & Höcker 2003), plane-wave destruction (Fomel 2002), and dynamic image warping (Arias 2016) have been proposed to estimate seismic reflection orientations or slopes. However, the latter two methods are not applicable to estimate stratigraphic orientations. In this paper, I use the structure tensor method to estimate orientations of both structural features (reflectors) and stratigraphic features (channels).

### 2.1 Structure tensors

A structure tensor (e.g. Van Vliet & Verbeek 1995; Weickert 1997; Fehmers & Höcker 2003) at each seismic image sample can be constructed as a smoothed outer product of image gradient $\mathbf{g}$ at that sample:

$$\mathbf{T} = \langle \mathbf{g}\mathbf{g}^\top \rangle, \tag{1}$$

where $\langle \cdot \rangle$ denotes smoothing for each element of the outer-product or structure tensor. This smoothing, often implemented as a Gaussian filter, helps to construct structure tensors with stable estimations of seismic structural and stratigraphic orientations.

For a 2-D image, each structure tensor $\mathbf{T}$ is a $2 \times 2$ symmetric positive-semi-definite matrix

$$\mathbf{T} = \langle \mathbf{g}\mathbf{g}^\top \rangle = \begin{bmatrix} \langle g_1 g_1 \rangle & \langle g_1 g_2 \rangle \\ \langle g_1 g_2 \rangle & \langle g_2 g_2 \rangle \end{bmatrix}, \tag{2}$$

where $\mathbf{g} = [g_1\ g_2]$ represent 2-D image gradients with first derivatives computed in vertical ($g_1$) and horizontal ($g_2$) directions. As shown by Fehmers & Höcker (2003), seismic reflector orientation at each image sample can be estimated from the eigen-decomposition of the structure tensor $\mathbf{T}$ at that sample

$$\mathbf{T} = \lambda_u \mathbf{u}\mathbf{u}^\top + \lambda_v \mathbf{v}\mathbf{v}^\top, \tag{3}$$

where $\lambda_u$ and $\lambda_v$ are the eigenvalues corresponding to eigenvectors $\mathbf{u}$ and $\mathbf{v}$ of $\mathbf{T}$. If we label the eigenvalues $\lambda_u \geq \lambda_v \geq 0$, then the corresponding eigenvectors $\mathbf{u}$ are perpendicular to locally linear features (seismic reflections) in an image, and the eigenvectors $\mathbf{v}$ are parallel to such features. The eigenvalues $\lambda_u$ and $\lambda_v$ indicate the isotropy and linearity of structures apparent in the image (Fehmers & Höcker 2003; Hale 2009b). If $\lambda_u \approx \lambda_v$, the structure is almost isotropic and there is not preferred orientation. If $\lambda_u \gg \lambda_v$, the structure is anisotropic with large linearity.

For a 3-D image, each structure tensor $\mathbf{T}$ is a $3 \times 3$ symmetric positive-semi-definite matrix

$$\mathbf{T} = \langle \mathbf{g}\mathbf{g}^\top \rangle = \begin{bmatrix} \langle g_1 g_1 \rangle & \langle g_1 g_2 \rangle & \langle g_1 g_3 \rangle \\ \langle g_1 g_2 \rangle & \langle g_2 g_2 \rangle & \langle g_2 g_3 \rangle \\ \langle g_1 g_3 \rangle & \langle g_2 g_3 \rangle & \langle g_3 g_3 \rangle \end{bmatrix}, \tag{4}$$

where $g_1$, $g_2$, and $g_3$ are the three components of an image gradient vector $\mathbf{g}$ computed at a 3-D image sample. The eigen-decomposition of such a 3-D structure tensor is as follows:

$$\mathbf{T} = \lambda_u \mathbf{u}\mathbf{u}^\top + \lambda_v \mathbf{v}\mathbf{v}^\top + \lambda_w \mathbf{w}\mathbf{w}^\top. \tag{5}$$

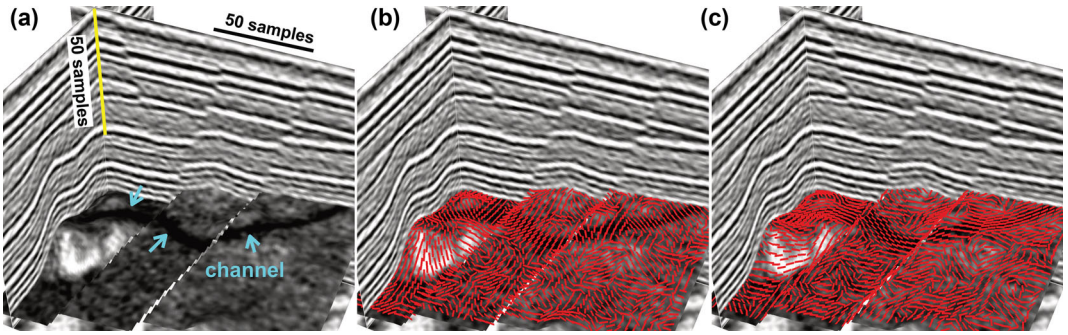


**Figure 1.** (a) A 3-D seismic image is displayed with a horizon surface, which is picked by following seismic reflectors. The eigenvectors (yellow segments) (b) **v** and (c) **w** of structure tensors are aligned within the horizon surface and are perpendicular and parallel to the channel, respectively. These vectors are estimated directly from the seismic image without picking the horizon.

Similarly, we label the eigenvalues and corresponding eigenvectors so that $\lambda_u \geq \lambda_v \geq \lambda_w$.

As discussed by Hale (2009b), the eigenvectors **u**, corresponding to the largest eigenvalues $\lambda_u$, are orthogonal to linear or planar features. Both eigenvectors **v** and **w** lie within the planes of any planar features (seismic reflections), and indicate orientations of stratigraphic features such as channels apparent within the planes. As shown in Fig. 1(a), the horizon surface is picked following the locally planar reflections, and a channel (denoted by cyan arrows) is apparent on the surface. The eigenvectors **v** and **w** are aligned within the horizon surface as denoted by the yellow segments in Figs 1(b) and (c). Near the seismic channel, we observe that eigenvectors **v** are orthogonal to the channel while the eigenvectors **w** are parallel to the channel. Away from the channel, the eigenvectors **v** and **w** are arbitrarily oriented but still aligned within the horizon surface. Although I display the eigenvectors **v** and **w** only on the extracted horizon surface, I actually estimate the vectors for all image samples in the 3-D seismic image. I estimate these vectors directly from the 3-D seismic image using structure tensors (eq. 5) without first extracting horizon surfaces.

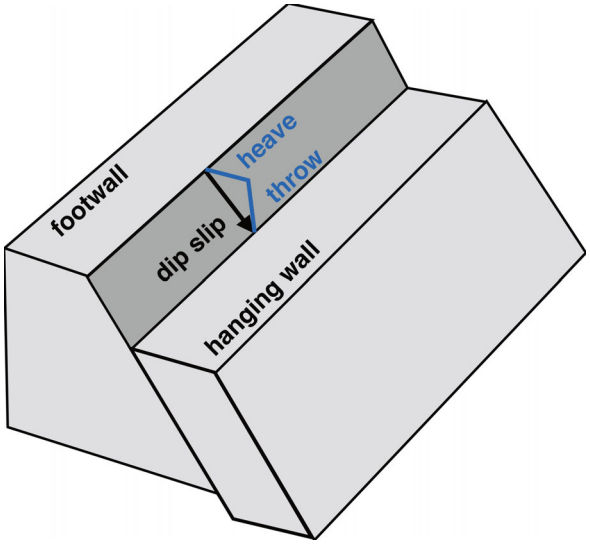


**Figure 2.** Fault dip slip is a vector representing fault displacement in the dip direction. Fault throw is the vertical component of the slip.

## 3 FAULT SLIPS

Fault is another common type of geologic structure that represents discontinuity of subsurface rock properties. Across a fault, there are significant displacements due to the movement of the hanging wall and footwall blocks on the opposite sides of the fault. Fault slip is defined as the displacement vector of the hanging wall block relative to the footwall block. Such fault slips are often spatially variant along a fault surface in both fault strike and dip directions. To extend information across a fault in geophysical inversion, we have to first estimate the fault slip vectors which tell us how to correlate rock properties across the fault.

Similar to the structural and stratigraphic orientations, we can also estimate fault slip vectors from a seismic image. In a seismic image, faults represent discontinuities of seismic reflectors and fault slips represent displacement vectors of the reflectors across the faults. As discussed by Wu & Hale (2016), fault strike slips are typically less apparent than dip slips in a 3-D seismic image. Therefore, we often can estimate only fault dip slips from a seismic image. As shown in Fig. 2, fault dip slip is a displacement vector, in the dip direction, of the hanging wall side of a fault relative to the footwall side.

To estimate fault dip slips, I first use the methods discussed by Wu & Hale (2016) to extract fault surfaces (Fig. 3b) from a seismic image (Fig. 3a). As discussed in detail by Wu & Hale (2016), I then estimate fault slips by correlating seismic reflectors on the footwall and hanging wall sides of each fault surface using the dynamic image warping method (Hale 2013a). While estimating all the vertical, inline, and crossline components of fault slip vectors, I display only the vertical components (fault throws) on the fault surface in Fig. 3(b). We observe that the estimated fault throws are spatially variant along each fault surface. I verify the estimated fault slips by using them in an unfaulting method (Wu *et al.* 2016) to compute an unfaulted image in Fig. 3(c). We can observe that the seismic reflectors across faults are correctly relocated after removing the faulting in the seismic image using the estimated slips, which indicates that the estimated fault slips are accurate enough to correlate reflectors across the faults.

## 4 REGULARIZATION

After estimating fault slips and orientations of seismic structural and stratigraphic features, I then use a simple example of seismic impedance inversion to explain the structure-, stratigraphy- and fault-guided regularization. Seismic impedance inversion often requires first estimating a proper seismic wavelet. To simplify the formulation of the inversion problem and avoid uncertainties due to the wavelet estimation, I assume the wavelet is known and a seismic reflectivity image is computed by deconvolving the seismic amplitude image using the wavelet.

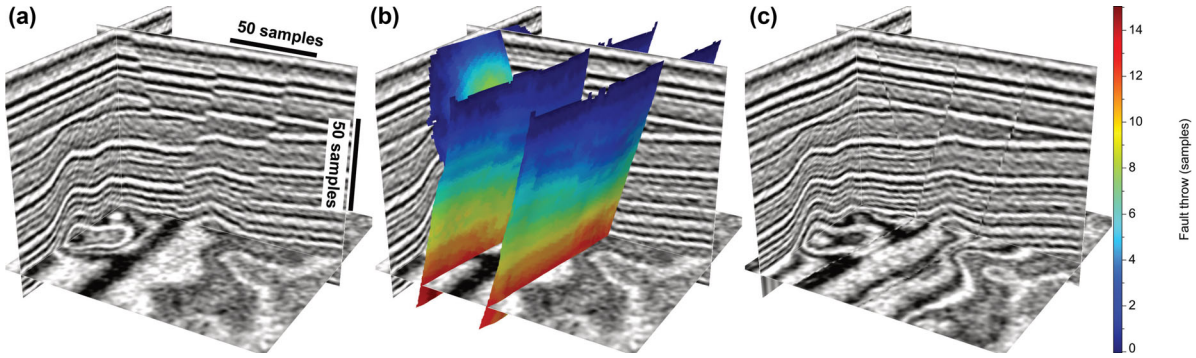


**Figure 3.** (a) A 3-D seismic image is displayed with (b) fault surfaces coloured by fault throws which are vertical components of estimated fault slip vectors. The fault slips are verified by using them to (c) remove the faulting in the seismic image.

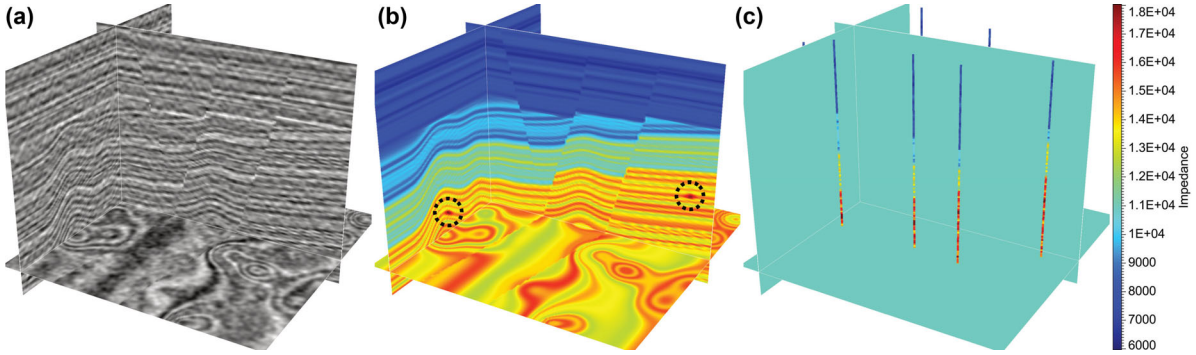


**Figure 4.** A 3-D view of the noisy (a) reflectivity, (b) true impedance, and (c) an initial impedance model with known values at well logs but zero values elsewhere.

As a 3-D synthetic example, Fig. 4(a) shows a 3-D reflectivity image computed from the noisy seismic amplitude image shown in Fig. 3(a) or 1(a). Fig. 4(b) is the corresponding true impedance model including three faults and a stratigraphic channel with relatively high impedance values as highlighted by the black cycles.

### 4.1 Forward modelling

In this simplified impedance inversion from seismic reflectivities, the forward modelling is simply as follows according to Russell *et al.* (2006):

$$\frac{1}{2}(\ln p_{i+1} - \ln p_i) \approx r_i, \tag{6}$$

where $p_i$ represents the unknown impedance at $i$th sample of a seismic trace, and $r_i$ represent the known reflectivity at that sample. Let $z_i = \frac{1}{2}\ln p_i$, we can further simplify eq. (6) as follows:

$$z_{i+1} - z_i \approx r_i. \tag{7}$$

In this problem, the forward operator is simply vertical differentiation that is applied to each trace of a 3-D model $z(\mathbf{x})$ independently:

$$\Delta_1 z(\mathbf{x}) \approx r(\mathbf{x}), \tag{8}$$

where $\Delta_1$ represents the vertical differentiation (forward operator) and $\mathbf{x}$ represents 3-D coordinates. $z(\mathbf{x})$ represents a 3-D impedance model to be estimated and $r(\mathbf{x})$ is the known noisy reflectivity data (Fig. 4a). Let $\mathbf{F} = \Delta_1$ represents the forward operator, we can formulate eq. (8) as a general form of a geophysical inversion problem

$$\mathbf{F}z(\mathbf{x}) \approx r(\mathbf{x}). \tag{9}$$

### 4.2 Structure- and stratigraphy-guided regularization

As the forward operator $\mathbf{F}$ in eq. (9) represents vertical differentiation, directly solving this equation is equivalent to vertically integrating the known noisy reflectivity data trace by trace. The integration may be unstable because of the noise, and errors may propagate vertically along the integration path. Also the solution may be laterally discontinuous or inconsistent by independently integrating trace by trace. Similar to all geophysical inversion problems, regularization can be imposed on the model ($z(\mathbf{x})$ in eq. 9) to obtain a more stable and smooth solution. One way of imposing smoothness on the model is to let the gradients of the model approximately equal to zeros and solve the following regularized problem:

$$\begin{aligned} \mathbf{F}z(\mathbf{x}) &\approx r(\mathbf{x}) \\ \nabla z(\mathbf{x}) &\approx \mathbf{0}, \end{aligned} \tag{10}$$

where $\nabla$ represents the gradient operator.

By assuming the gradients (derivatives in inline, crossline, and vertical directions) of the model approximately equal to zeros, we are actually imposing isotropic smoothness on the model. However, the seismic impedance, similar to all other rock property models, is typically not isotropic. The property values of a subsurface model may vary slowly in lateral directions along structures but can vary rapidly in directions perpendicular to such structures.

Therefore, instead of the isotropic regularization in eq. (11), we may want to impose anisotropic structure- and stratigraphy-guided regularization on the model as follows:

$$\begin{aligned} \mathbf{F}z(\mathbf{x}) &\approx r(\mathbf{x}) \\ \mathbf{u}^\top \nabla z(\mathbf{x}) &\approx \mathbf{0} \end{aligned}$$

$$\mathbf{v}^\top \nabla z(\mathbf{x}) \approx \mathbf{0}$$
$$\mathbf{w}^\top \nabla z(\mathbf{x}) \approx \mathbf{0}. \tag{11}$$

As discussed above, $\mathbf{u}(\mathbf{x})$, $\mathbf{v}(\mathbf{x})$, and $\mathbf{w}(\mathbf{x})$ are eigenvectors computed from the eigen-decomposition of 3-D seismic structure tensors. These eigenvectors are computed for all samples $\mathbf{x}$ in a 3-D seismic image. The eigenvectors $\mathbf{u}$ are orthogonal to linear or planar features (seismic reflectors). Both eigenvectors $\mathbf{v}$ and $\mathbf{w}$ lie within the planes of any planar features, and indicate orientations of stratigraphic features such as channels apparent within the planes. More specifically, the vectors $\mathbf{v}$ are orthogonal to stratigraphic features and $\mathbf{w}$ are parallel to such features as shown in Figs 1(b) and (c), respectively. $\mathbf{u}^\top\nabla$, $\mathbf{v}^\top\nabla$, and $\mathbf{w}^\top\nabla$ represent directional derivatives in directions along the vectors $\mathbf{u}$, $\mathbf{v}$, and $\mathbf{w}$, respectively.

By setting the directional derivatives of the model to be approximately zeros, we are actually imposing smoothness on the model in directions along the vectors $\mathbf{u}$, $\mathbf{v}$ and $\mathbf{w}$. We can also impose different extents of smoothness on the model in different directions by weighting the regularization terms

$$\begin{aligned}\mathbf{F}z(\mathbf{x}) &\approx r(\mathbf{x})\\ \mu_u\mathbf{u}^\top\nabla z(\mathbf{x}) &\approx \mathbf{0}\\ \mu_v\mathbf{v}^\top\nabla z(\mathbf{x}) &\approx \mathbf{0}\\ \mu_w\mathbf{w}^\top\nabla z(\mathbf{x}) &\approx \mathbf{0}.\end{aligned} \tag{12}$$

These weights can be either constants or spatially variant quality maps. For example, a seismic impedance model, as the one shown in Fig. 4(a), varies slowly in lateral directions ($\mathbf{v}$ and $\mathbf{w}$) along structures but vary rapidly in directions ($\mathbf{u}$) perpendicular to the structures. Therefore, in this case, we can set the weights $\mu_u$ to be nearly zeros but set $\mu_v$ and $\mu_w$ with high values (close to ones).

### 4.3 Fault-guided regularization

With the structure- and stratigraphy-guided regularization, we are imposing smoothness on a model in directions along seismic structural and stratigraphic features. However, property values of a subsurface model are not always smooth and continuous along the structural and stratigraphic features, they are discontinuous across faults, like the impedance values in Fig. 4(b). One way to preserve property discontinuities at faults in a model is to first detect the fault positions, and then set zero values at the fault positions in the weighing maps $\mu_u$, $\mu_v$, and $\mu_w$ to stop smoothness constraints at the faults.

In this way, we are able to preserve discontinuities at faults, but also prevent property information on opposite sides of faults from spreading across the faults. The property values on opposite sides of faults are discontinuous but are correlated by fault slips vectors. Therefore, a better way of dealing with faults is to add fault slip constrained regularization to the model as follows:

$$\begin{aligned}\mathbf{F}z(\mathbf{x}) &\approx r(\mathbf{x})\\ \mu_u\mathbf{u}^\top\nabla z(\mathbf{x}) &\approx \mathbf{0}\\ \mu_v\mathbf{v}^\top\nabla z(\mathbf{x}) &\approx \mathbf{0}\\ \mu_w\mathbf{w}^\top\nabla z(\mathbf{x}) &\approx \mathbf{0}\\ \mu_s\beta\left[z(\mathbf{x}_h) - z(\mathbf{x}_f)\right] &\approx \mathbf{0},\end{aligned} \tag{13}$$

where $\mu_s$ represents a weight for the fault-guided regularization term and often is a constant. $\beta$ is another constant scale used to balance the fault-guided regularization with the other equations. In most cases, I use $\beta = \frac{N}{L}$, where $N$ represents the number of samples in the model while $L$ represents the number of samples on the faults. $\mathbf{x}_h$ represent locations of samples adjacent to a fault from the its hanging wall side, while $\mathbf{x}_f$ represent locations of corresponding samples adjacent to the fault from its footwall side. Given any sample $\mathbf{x}_h$ located at the hanging wall side, we can find the corresponding correlated sample at the footwall side using the estimated fault slip vector $\mathbf{s}(\mathbf{x}_h)$ at $\mathbf{x}_h$: $\mathbf{x}_f = \mathbf{x}_h - \mathbf{s}(\mathbf{x}_h)$. This fault-guided regularization term means that we expect the model property values of the correlated samples on opposite sides of faults to be approximately equal. At the points $\mathbf{x}_h$ and $\mathbf{x}_f$ where the fault-guided regularization is defined, the structure- and stratigraphy-guided regularization is turned off by setting $\mu_u = \mu_v = \mu_w = 0$ to stop the smoothness constraints near the faults. Using this regularization, we are able to spread property information across faults while preserving the property discontinuities at the faults. With this regularization, we assume that the rock layers across faults are geologically consistent following fault slips. For some growth faults where the layers across faults cannot be correlated, we might want to stop spreading property information across faults by simply setting $\mu_u = \mu_v = \mu_w = 0$ at faults.

### 4.4 Least-squares solution

Letting $\mathbf{M}$ represent the scaled differentiation operator $(\mu_s\beta[z(\mathbf{x}_h) - z(\mathbf{x}_f)])$ applied only to the samples adjacent to faults, we can rewrite the above eq. (13) in a simpler form as follows:

$$\begin{aligned}\mathbf{F}z(\mathbf{x}) &\approx r(\mathbf{x})\\ \mu_u\mathbf{u}^\top\nabla z(\mathbf{x}) &\approx \mathbf{0}\\ \mu_v\mathbf{v}^\top\nabla z(\mathbf{x}) &\approx \mathbf{0}\\ \mu_w\mathbf{w}^\top\nabla z(\mathbf{x}) &\approx \mathbf{0}\\ \mathbf{M}z(\mathbf{x}) &\approx \mathbf{0}.\end{aligned} \tag{14}$$

With the extra structure-, stratigraphy-, and fault-guided regularization terms, we now have more equations than unknowns as in eq. (14). Therefore, we can compute a least-squares solution of these equations by solving the corresponding normal equation:

$$\left(\mathbf{F}^\top\mathbf{F} + \nabla^\top\mathbf{D}\nabla + \mathbf{M}^\top\mathbf{M}\right)z(\mathbf{x}) = \mathbf{F}^\top r(\mathbf{x}), \tag{15}$$

where $\mathbf{D} = \mu_u^2\mathbf{u}\mathbf{u}^\top + \mu_v^2\mathbf{v}\mathbf{v}^\top + \mu_w^2\mathbf{w}\mathbf{w}^\top$ is an anisotropic tensor field which has exactly the same eigenvectors as those in the 3-D structure tensors (eq. 5). However, the corresponding eigenvalues are replaced with specified weights $\mu_u^2$, $\mu_v^2$, and $\mu_w^2$.

The above inversion with structure-, stratigraphy- and structure-guided regularization contains three parts:

**Structure-, stratigraphy- and fault-guided inversion**

(i): forward modelling

$$\mathbf{F}^\top\mathbf{F}z(\mathbf{x}) = \mathbf{F}^\top r(\mathbf{x}) \tag{16}$$

(ii): structure- and stratigraphy-guided regularization

$$\nabla^\top\mathbf{D}\nabla z(\mathbf{x}) = \mathbf{0} \tag{17}$$

(iii): fault-guided regularization

$$\mathbf{M}^\top\mathbf{M}z(\mathbf{x}) = \mathbf{0} \tag{18}$$

The first part contains the forward modelling operator $\mathbf{F}$. The second part is structure- and stratigraphy-guided regularization which simply includes the gradient operator ($\nabla$) and an anisotropic tensor field ($\mathbf{D}$) constructed from the eigenvector of seismic structure tensors and some specified weights. With this tensor field, the anisotropic

smoothness constraints imposed on the model are structure- and stratigraphy-oriented. We are able to conveniently impose different extents of the anisotropic smoothness in different orientations by varying the corresponding weights $\mu_u$, $\mu_v$ and $\mu_w$. In most cases, we can simply set these weights to be constant values in the range between 0 and 1 to specify the strength of smoothness in directions of vectors **u**, **v**, and **w**. In practice, the subsurface rock properties often extend more smoothly and continuously in directions parallel (vectors **v** and **w**) to structural and stratigraphic features than in directions perpendicular to such features. Based on this observation, we should set $\mu_u$ to be nearly zero while set $\mu_v$ and $\mu_w$ to be close to one in most geophysical inversion problems to obtain subsurface models conforming to structural and stratigraphic features. These weights $\mu_u$, $\mu_v$, and $\mu_w$ can also be set as mappings with spatially variant values in the range between 0 and 1 to impose spatially variant and anisotropic smoothness regularization in geophysical inversion. In practice, such mappings can be computed as isotropy or linearity and planarity (Hale 2009b; Wu 2017) of seismic reflections in a seismic image. In areas with lower isotropy or higher linearity and planarity, we should set smaller $\mu_u$ but larger $\mu_v$ and $\mu_w$ in these areas to impose stronger smoothness in directions of vectors **v** and **w**. In areas with higher isotropy or lower linearity and planarity, we should set $\mu_u$, $\mu_v$ and $\mu_w$ to be approximately equal to impose isotropic smoothness in these areas. More discussions of choosing spatially constant or variant weights will be discussed in synthetic and real examples.

The third part is the fault-guided regularization which contains a simple differentiation operator applied only to the samples adjacent to faults. By solving these three parts simultaneously as in eq. (15), we are able to obtain an inverted model conforms to faults and structural and stratigraphic features. As the matrices in the eq. (15) are symmetric positive definite, we can solve the linear system using the Conjugate Gradient (CG) method.

### 4.5 Constraints from well logs

Geophysical inversion often also requires a starting model. A proper initial model can be helpful to reduce uncertainties in the inversion and may accelerate the convergence of the inversion process. Such an initial model can be interpolated from well-log measurements. Hale (2009a, 2010) proposes an image-guided interpolation method to compute a subsurface model that conforms to both seismic structures and well-log measurements.

With structure-, stratigraphy-, and fault-guided regularization, we do not need to first interpolate an initial model conforms to structures and well-log measurements. These regularization terms will spread the well-log measurements away from well positions to the whole volume along structural and stratigraphic features and across faults. Therefore, we can combine the initial model interpolation and the inversion into one step by solving the following problem of structure-, stratigraphy- and fault-guided inversion with hard constraints from well-log measurements.

In the forth part of constraints, $\{f_k, k = 1, 2, \ldots, m\}$ represent a set of $m$ known values which can be rock property values measured in well logs. $\mathbf{x}_k$ represent positions of the $m$ known values. As discussed previously, by solving the first three parts (i, ii and iii) simultaneously, we compute a solution of structure-, stratigraphy- and fault-guided inversion. If we solve the second three parts (ii, iii and iv) simultaneously, we actually compute a structure-, stratigraphy-, and fault-guided interpolation of the known values. As discussed by Hale (2009a), solving the second part and the forth part simultaneously yields an image-guided harmonic interpolation. With the constraint equation (the forth part), we expect the interpolant $z(\mathbf{x})$ to be equal to the known values $z(\mathbf{x}_k) = f_k$ at the know positions $\mathbf{x}_k$. With the equation of structural and stratigraphic regularization (second part), we expect the directional derivatives of the interpolant $z(\mathbf{x})$ in structural and stratigraphic orientations to be approximately zeros. Solving these two equations simultaneously, we are able to extend the known values smoothly along the structural and stratigraphic orientations to compute a structure- and stratigraphy-guided interpolation.

**Structure-, stratigraphy- and fault-guided inversion with constraints**

(i): forward modelling

$$\mathbf{F}^\top\mathbf{F}z(\mathbf{x}) = \mathbf{F}^\top r(\mathbf{x}) \tag{19}$$

(ii): structure- and stratigraphy-guided regularization

$$\nabla^\top\mathbf{D}\nabla z(\mathbf{x}) = \mathbf{0} \tag{20}$$

(iii): fault-guided regularization

$$\mathbf{M}^\top\mathbf{M}z(\mathbf{x}) = \mathbf{0} \tag{21}$$

(iv): hard constraints

$$\text{subject to } z(\mathbf{x}_k) = f_k,\ k = 1, 2, \ldots, m \tag{22}$$

The constraints of known properties often can only provide local control in the inversion because those properties are often measured only at limited positions. The structure-, stratigraphy-, and fault-guided regularization is helpful to provide a more global control by spreading the measured properties across faults and along structural and stratigraphic features. By combining all the above four part together, we solve a following constrained linear system:

$$\left(\mathbf{F}^\top\mathbf{F} + \nabla^\top\mathbf{D}\nabla + \mathbf{M}^\top\mathbf{M}\right)z(\mathbf{x}) = \mathbf{F}^\top r(\mathbf{x})$$
$$\text{subject to } z(\mathbf{x}_k) = f_k,\ k = 1, 2, \ldots, m. \tag{23}$$

This constrained linear system combines the interpolation and the inversion, both of which are guided by fault slips and structural and stratigraphic orientations.

I solve this constrained linear system using a preconditioned CG method (Wu & Hale 2015; Wu *et al.* 2016). The constraint equation $z(\mathbf{x}_k) = f_k,\ k = 1, 2, \ldots, m$ is implemented with simple pre-conditioners in the CG method; the details of constructing such pre-conditioners are discussed by Wu & Hale (2015). In this preconditioned CG method, I choose a simple initial model with zero values everywhere but known values $f_k$ at $\mathbf{x}_k$, which obviously satisfies the constraint equation. Beginning with such an initial model that satisfies the constraint equation, the CG iterations gradually update the function for all samples, while the pre-conditioners guarantee that the updated function always satisfies the constraint equation after each iteration.

### 4.6 Results

Fig. 4 shows the 3-D synthetic example I use to illustrate the regularization and the hard constraints from well logs. This example contains three faults (Fig. 3b) and a channel with relatively high impedance values as denoted by black circles in the true impedance model (Fig. 4b). Fig. 4(a) shows a noisy reflectivity image computed by devolving the corresponding seismic image (Figs 1a and 3a) with a known wavelet. The goal of this example is to invert an impedance model from this noisy reflectivity image with constraints of the known impedance values recorded at the 7 well logs shown in Fig. 4(c).

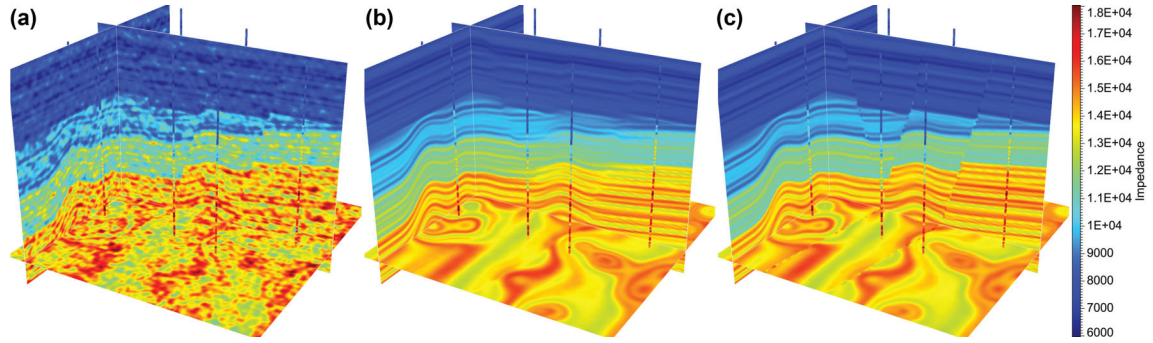


**Figure 5.** (a) Estimated impedance model with $\mu_u = 0.001$ and $\mu_v = \mu_w = \mu_s = 0.1$. (b) Estimated impedance model with $\mu_u = 0.001$, $\mu_v = \mu_w = 0.9$, and $\mu_s = 0.0$. (c) Estimated impedance model with $\mu_u = 0.001$ and $\mu_v = \mu_w = \mu_s = 0.9$.

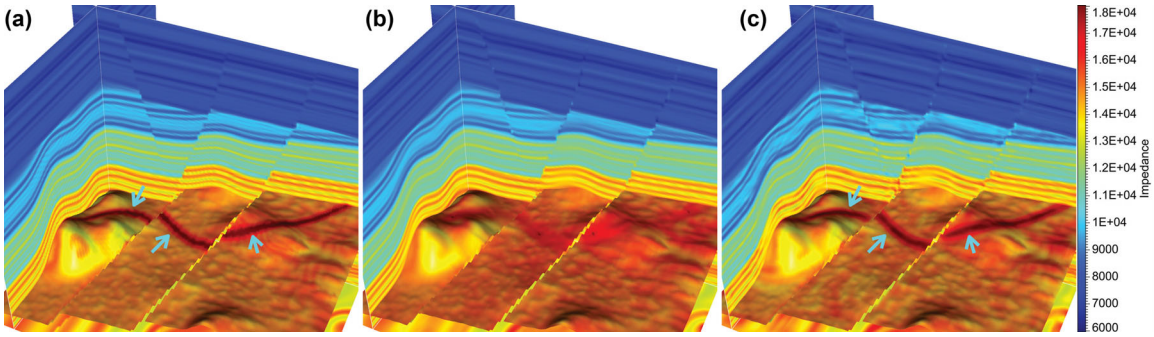


**Figure 6.** (a) True impedance model. (b) Estimated impedance model with $\mu_u = 0.001$ and $\mu_v = \mu_w = \mu_s = 0.9$. (c) Estimated impedance model with $\mu_u = 0.001$, $\mu_v = 0.01$ and $\mu_w = \mu_s = 0.9$. The channel (denoted by cyan arrows) with relatively high impedance values is smoothed out in (b) but is preserved in (c).

In this example, I first estimate structural and stratigraphic orientations from the seismic image (Figs 1a and 3a) using structure tensors (eq. 5). From the eigen-decomposition of the structure tensors, I obtain three eigenvectors **u**, **v**, and **w** with corresponding three eigenvalues $\lambda_u \geq \lambda_v \geq \lambda_w$. As discussed previously in this paper, the eigenvectors **u** are orthogonal to linear or planar features. Both eigenvectors **v** and **w** lie within the planes of any planar features (seismic reflections), and indicate orientations of stratigraphic features such as channels apparent within the planes. As shown in Figs 1(b) and (c), the vectors **v** and **w** are aligned within the horizon surface which is extracted following seismic reflectors. Moreover, vectors **v** (Fig. 1b) are orthogonal to channel and **w** (Fig. 1c) are parallel to the channel. In areas without stratigraphic features, the image features on the horizon surface are isotropic and the eigenvectors **v** and **w** are arbitrarily oriented as shown in Figs 1(b) and (c).

I also extract fault surfaces from the 3-D seismic image (Fig. 3b) and estimate fault slips on the surfaces. Fault slips are vectors with inline, crossline, and vertical components. I display only the vertical components (fault throws) on the fault surfaces shown in Fig. 3(b). To verify the estimated faults slip vectors, I use them to remove the faulting the original seismic image (Fig. 3a) and obtain an unfaulted image (Fig. 3c). In this unfaulted image, seismic reflectors are relocated across faults, which indicates that the estimated fault slips are accurate enough to correlate seismic reflectors across the faults.

With the estimated structural and stratigraphic orientations (**u**, **v** and **w**) and the fault slip vectors ($\mathbf{s}(\mathbf{x}_h)$), I construct regularization terms as in eq. (13) for the seismic impedance inversion. In general, a impedance model varies slowly along structural and stratigraphic features in directions along the vectors **v**, and **w** but likely varies rapidly in directions along the vectors **u** which are perpendicular to such features. Therefore, when constructing regularization for imposing smoothness on the model, I set $\mu_u = 0.001$ to impose weak smoothness in the directions of vectors **u** for all tests (Figs 5 and 6) in this 3-D synthetic example.

In all these tests shown in Figs 5 and 6, I begin with an initial impedance model with known values at well-log positions and zero values elsewhere and solve the constrained linear system (eq. 23) using a preconditioned CG method. However, for each test, I set different weights $\mu_v$, $\mu_w$ and $\mu_s$ in constructing the regularization terms $\nabla^{\mathsf{T}}\mathbf{D}\nabla$ and $\mathbf{M}^{\top}\mathbf{M}$ in eq. (23).

In computing the impedance model shown in Fig. 5(a), I set $\mu_v = \mu_w = \mu_s = 0.1$ which means that I impose weak smoothness on the model in all directions along structural and stratigraphic features and across faults. We observe that the estimated impedance model (Fig. 5a) is noisy because of the noisy input reflectivity data (Fig. 4a).

In computing the impedance model shown in Fig. 5(b), I set $\mu_v = \mu_w = 0.9$ and $\mu_s = 0.0$ which means that I impose strong smoothness on the model in directions along structures but impose no constraints on the model across faults. With these settings for the regularization, I obtain a much cleaner impedance model (Fig. 5b) with more continuous values along structures comparing to the estimated model with weaker smoothness regularization (Fig. 5a). However, if we compare this estimated model (Fig. 5b) with the true impedance model (Fig. 4b), we observe that the discontinuities at the fault positions are not preserved because of the smoothness regularization along structures.

In computing the impedance model shown in Fig. 5(c), I set $\mu_v = \mu_w = \mu_s = 0.9$ which means that I impose strong smoothness on the model in directions along structures and also impose strong fault-guided regularization on the model across faults. With all these regularization, I obtain an estimated model (Fig. 5c) which

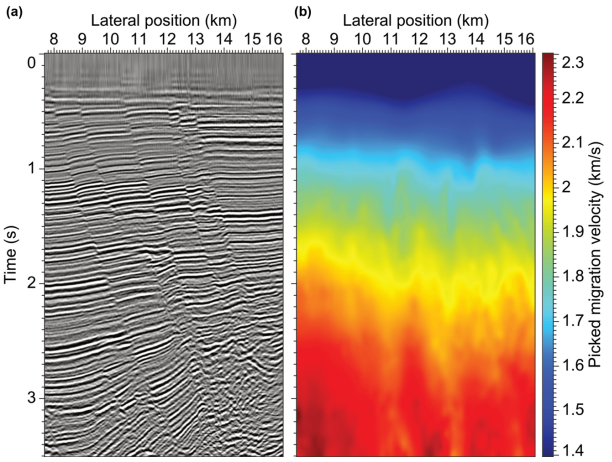


**Figure 7.** (a) 2-D time-migrated image. (b) The corresponding migration velocity from automatic picking. Both of the images are reproduced from the paper published by Fomel (2007).

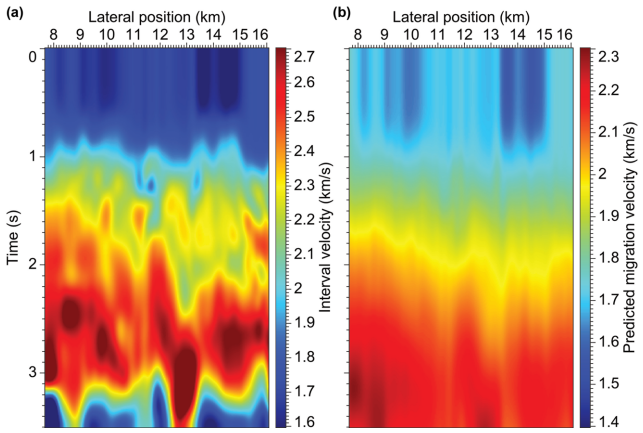


**Figure 8.** (a) Estimated interval velocity using shaping regularization with triangle local plane-wave smoothing. (b) Predicted migration velocity computed from the estimated interval velocity. Both the results are reproduced from the paper published by Fomel (2007).

is smooth and continuous along structures but discontinuous at faults, as expected. This estimated model is visually close to the true impedance model shown in Fig. 4(b). However, one problem of this estimated model is that the stratigraphic features (channel) are smoothed out as shown in Fig. 6(b) because of the strong smoothness regularization along directions of vectors **v** which are orthogonal to the stratigraphic features.

Therefore, in computing the impedance model shown in Fig. 6(c), I set $\mu_v = 0.01$ and $\mu_w = \mu_s = 0.9$ to impose strong regularization on the model only in directions along stratigraphic features and across faults. By doing this, we decrease the smoothness constraints on the model in directions orthogonal to channel and therefore preserve the relatively high impedance values on the channel as shown in Fig. 6(c). In this synthetic example, I directly use the well-log impedances as constraints to compute an impedance model. In practice, we might want to use only the low-frequency components of the well-log impedances as constraints in seismic impedance inversion to compensate the missing low frequencies in seismic data.

## 5 REAL EXAMPLES

Although the structure-, stratigraphy-, and fault-guided regularization is derived with the example of seismic impedance inversion, this regularization can be applied to other geophysical inversion problems. Below I use the regularization discussed above to estimate seismic interval velocity and compute structure- and stratigraphy-oriented semblance.

### 5.1 Velocity estimation

The first example is an application of structure- and fault-guided regularization in seismic velocity estimation. Fig. 7(a) shows a time-migrated seismic image of historic Gulf Mexico data set that I reproduce from the paper published by Fomel (2007). The corresponding migration velocity (Fig. 7b) is automatically picked from semblance gathers obtained in the process of velocity continuation (Fomel 2007). Again this velocity image is also reproduced from the paper published by Fomel (2007). The goal of this example is to estimate interval velocity from this picked time-migration velocity.

The picked time-migration (or root-mean-square) velocity and the interval velocity at each trace are related as follows according to Dix (1955)

$$C^2(\tau) = \frac{1}{\tau}\sum_i c_i^2 \Delta\tau_i, \tag{24}$$

where $C(\tau)$ is the picked time-migration velocity (Fig. 7b), $c_i$ is the interval velocity at each time sample, and $\tau$ is the vertical traveltime. Estimating the interval velocity from the time-migration velocity can be stated as computing a least-squares solution of the following equation (Valenciano *et al.* 2004)

$$\mathbf{WSc} \approx \mathbf{Wd}, \tag{25}$$

where **c** is the unknown vector of squared interval velocities, **d** is the known vector of squared time-migration velocities multiplied by the vertical traveltime, **S** is the causal integration operator, and **W** is a weighing matrix constructed from the confidence of the picked time-migration velocities.

To obtain an interval velocity image conforms to seismic structures, Fomel (2007) solve the above inversion problem (eq. 25) using the shaping regularization with triangle local plane-wave smoothing. Fig. 8(a) shows the estimated interval velocity image where some of the velocities do not truly follow the seismic structures. Moreover, the estimated interval velocity is smooth across faults where the velocity is expected to be discontinuous. Fig. 8(b) is the predicted migration velocity computed from the estimated interval velocity (Fig. 8a).

Next, I solve the same inversion problem but with structure- and fault-guided regularization discussed previously in this paper. From the seismic image (Fig. 7a), I first construct a tensor field $\mathbf{D}(\mathbf{x}) = \mu_u^2\mathbf{u}^\top\mathbf{u} + \mu_v^2\mathbf{v}^\top\mathbf{v}$ for the regularization $\nabla^\top\mathbf{D}\nabla$ using eigenvalues and eigenvectors of 2-D structure tensors (eq. 1). Instead of using constant weights $\mu_u$ and $\mu_v$ as in the previous 3-D synthetic example, in this example I define spatially variant weights using the spatially variant eigenvalues $\lambda_u(\mathbf{x})$ and $\lambda_v(\mathbf{x})$ ($\lambda_u(\mathbf{x}) \geq \lambda_v(\mathbf{x})$) as follows:

$$\mu_u(x) = \frac{\lambda_{\min} + \epsilon_0}{\lambda_v(\mathbf{x}) + \epsilon_0}, \quad \text{and} \quad \mu_v(x) = \frac{\lambda_{\min} + \epsilon_0}{\lambda_u(\mathbf{x}) + \epsilon_0}, \tag{26}$$

where $\lambda_{\min}$ is the minimum of the eigenvalues $\lambda_v(\mathbf{x})$: $\lambda_{\min} = \min_{\mathbf{x}}\{\lambda_v(\mathbf{x})\}$. The parameter $\epsilon_0$ is a small positive number used to

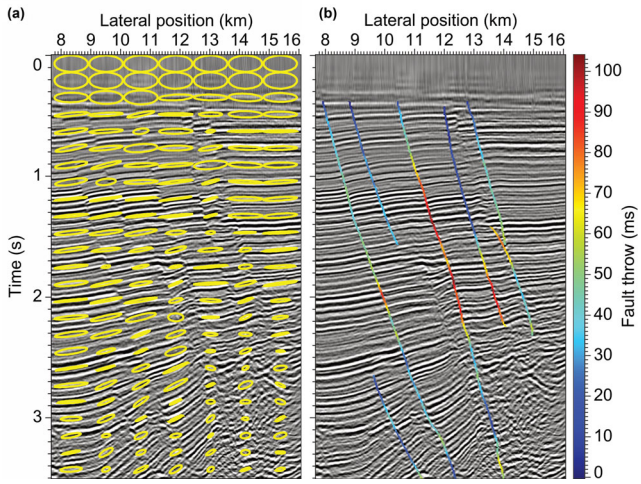


**Figure 9.** A 2-D seismic image is displayed with (a) tensors (yellow ellipses) and (b) fault throws, which are vertical components of fault slips estimated at fault positions. The tensors and fault slips are used to construct structure- and fault-guided regularization for the interval velocity estimation.

avoid dividing by zero in the above eq. (26). As $\lambda_u(\mathbf{x}) \geq \lambda_v(\mathbf{x}) \geq 0$, we have $0 \leq \mu_u(\mathbf{x}) \leq \mu_v(\mathbf{x}) \leq 1$.

The yellow ellipses in Fig. 9(a) shows some examples of the tensor field $\mathbf{D}(\mathbf{x})$ that I compute for all image samples by $\mathbf{D}(\mathbf{x}) = \mu_u^2 \mathbf{u}^\top \mathbf{u} + \mu_v^2 \mathbf{v}^\top \mathbf{v}$. The radii of the ellipses are scaled by $\mu_u$ and $\mu_v$. The major and minor axes of each ellipses are aligned in directions along vectors $\mathbf{v}$ (parallel to reflections) and $\mathbf{u}$ (perpendicular to reflections) because we have $\mu_v \geq \mu_u$. In the middle image area (Fig. 9a) with highly linear (anisotropic) structures, we have $\mu_v \gg \mu_u$ and therefore the major radii of the ellipses are much longer the minor radii. We observe the ellipses are aligned with the seismic reflections and are extremely narrow in the directions perpendicular to the reflections. In the top and right-bottom areas with isotropic structures, we have $\mu_v \approx \mu_u$ and therefore the major radii of the ellipses are nearly equal to the minor radii which makes the ellipses look like circles.

Using these spatially variant tensors to construct the structure-constraint regularization, I impose anisotropic smoothness on the model in areas where the structures are highly linear or anisotropic. Specifically, in these areas I impose strong smoothness in directions along structures but weak smoothness in perpendicular directions. In areas with isotropic structures, I actually impose isotropic smoothness on the model.

I also extract faults (Fig. 9b) from the seismic image and estimate fault slips on the extracted faults. In this 2-D case, fault slips are vectors with horizontal and vertical components. The vertical components are fault throws which are displayed in colour on the extracted faults as shown in Fig. 9(b). Relatively higher fault throws are displayed as red while lower throws are displayed as blue. We observe that the fault throws spatially vary with depth along the faults. The estimated fault positions and slips are used in fault-guided regularization to preserve discontinuities at faults and to spread information across faults in the model.

Using the computed tensor field (Fig. 9a) and fault slips (Fig. 9b), I construct structure- and fault-guided regularization for the velocity inversion problem (eq. 25) and estimate the interval velocity shown in Fig. 10(a). Fig. 10(b) shows the predicted migration velocity computed from the estimated interval velocity (Fig. 10b). Figs 11(a) and (b) show the seismic image overlaid with interval velocity images estimated by shaping regularization and structure-

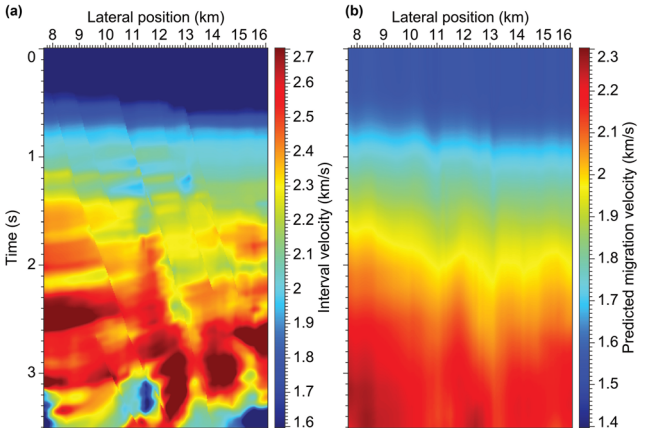


**Figure 10.** (a) Estimated interval velocity using structure- and fault-guided regularization. (b) Predicted migration velocity computed from the estimated interval velocity.

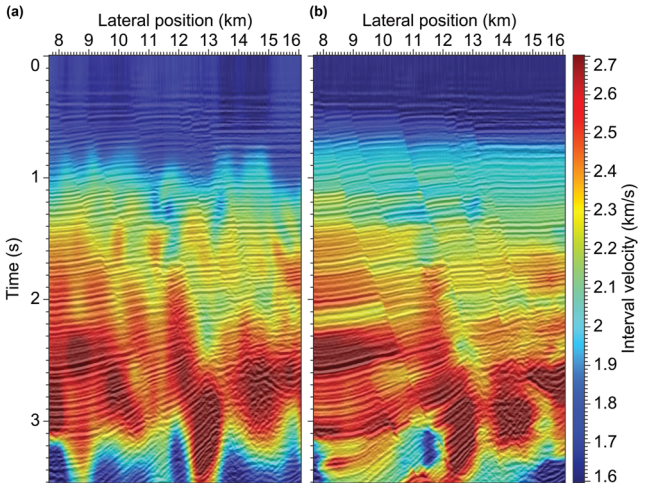


**Figure 11.** The seismic image from Fig. 7(a) is overlaid with interval velocity images estimated using (a) the shaping regularization and (b) structure- and fault-guided regularization.

and fault-guided regularization, respectively. We can observe that the interval velocity estimated using the structure- and fault-guided regularization is laterally more consistent with seismic structures than the one estimated using shaping regularization. Moreover, the velocity discontinuities are preserved using the fault-guided regularization as shown in Figs 10(a) and 11(b).

## 5.2 Semblance

The second example is to compute a semblance image from a 3-D seismic amplitude image shown in Fig. 12(a). Seismic semblance is a measure of lateral changes in a seismic image and therefore is useful to highlight faults and stratigraphic features from the seismic image (Marfurt *et al.* 1998). To better highlight faults and stratigraphic features, semblance is often computed along reflection dips (Marfurt *et al.* 1999). Such semblance is also defined as structure-oriented semblance (Hale 2013b):

$$s(\mathbf{x}) = \frac{\langle f(\mathbf{x}) \rangle^2}{\langle f(\mathbf{x})^2 \rangle}, \tag{27}$$

where $\langle \cdot \rangle$ denotes structure-oriented smoothing (Fehmers & Höcker 2003; Hale 2009b) of whatever is inside the brackets. As

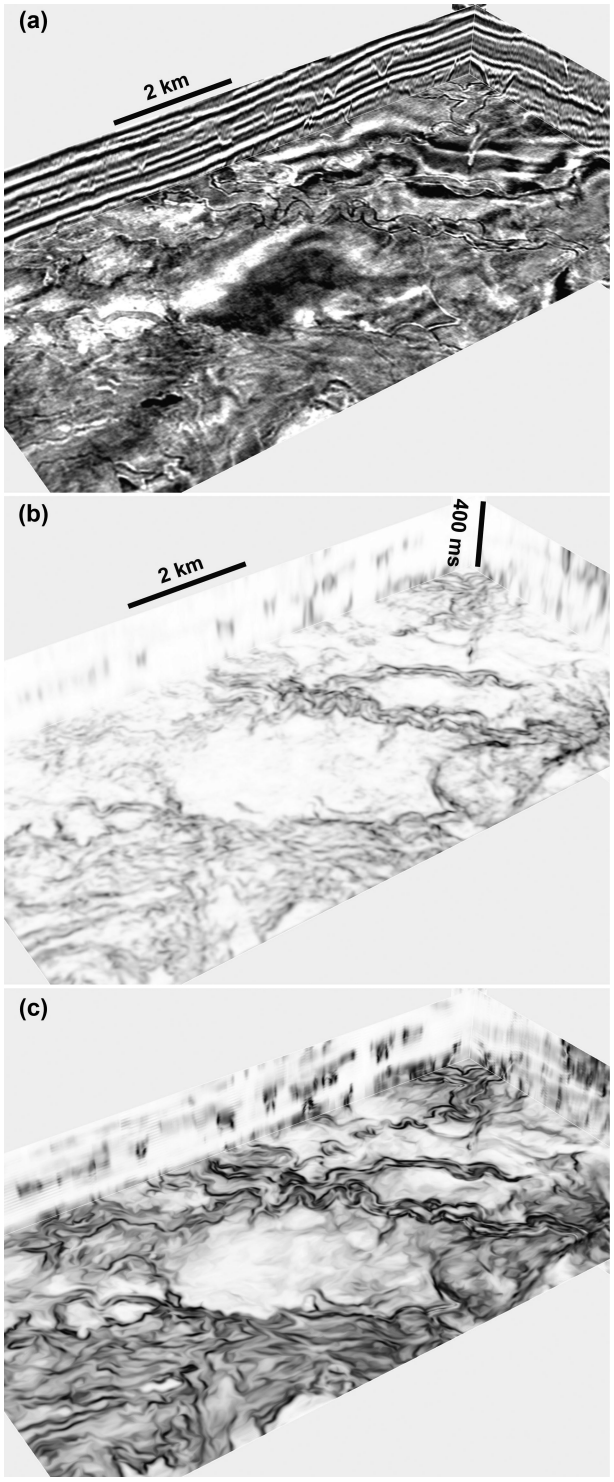


**Figure 12.** A 3-D view of a (a) seismic image, (b) planarity image, and (c) semblance image computed with structure- and stratigraphy-guided regularization.

discussed by Hale (2013b), the semblance ratios computed in this way will vary wildly where the denominators are small. To solve the problem of instability, Hale (2009b, 2013b) propose to an additional smoothing of numerators and denominators before computing the semblance ratios.

Here I consider the computation of semblance ratios as an inverse problem and using structure- and stratigraphy-guided regularization to compute stable semblance. Letting $a(\mathbf{x}) = \langle f(\mathbf{x})\rangle^2$ and $b(\mathbf{x}) = \langle f(\mathbf{x})^2\rangle$, I can formulate the semblance ratios as follows:

$$b(\mathbf{x})s(\mathbf{x}) = a(\mathbf{x}). \tag{28}$$

The semblance features, such as fault and stratigraphic features, typically extend in directions of vectors $\mathbf{u}$ (orthogonal to structures) and $\mathbf{w}$ (parallel to stratigraphic features) which are computed from seismic structure tensors. Therefore, I construct regularization with vectors $\mathbf{u}$ and $\mathbf{w}$ for the semblance computation:

$$\begin{aligned} b(\mathbf{x})s(\mathbf{x}) &\approx a(\mathbf{x}) \\ \mu_u \mathbf{u}^\top \nabla s(\mathbf{x}) &\approx \mathbf{0} \\ \mu_w \mathbf{w}^\top \nabla s(\mathbf{x}) &\approx \mathbf{0}. \end{aligned} \tag{29}$$

To detect faults which extend more vertically than laterally, we should impose stronger smoothness (larger $\mu_u$) on the semblance in directions along vectors $\mathbf{u}$. However, if we want to detect channels which extend more laterally than vertically, we should impose stronger smoothness (larger $\mu_w$) in directions along vectors $\mathbf{w}$. In this example, I set $\mu_u = 0.5$ and $\mu_w = 0.9$ to highlight stratigraphic features such as channels in the semblance image.

In addition to the regularization, we can also weight the semblance equation as follows:

$$\begin{aligned} q(\mathbf{x})b(\mathbf{x})s(\mathbf{x}) &\approx q(\mathbf{x})a(\mathbf{x}) \\ \mu_u \mathbf{u}^\top \nabla s(\mathbf{x}) &\approx \mathbf{0} \\ \mu_w \mathbf{w}^\top \nabla s(\mathbf{x}) &\approx \mathbf{0}, \end{aligned} \tag{30}$$

where the weighing map $q(\mathbf{x})$ is computed from a planarity image $p(\mathbf{x})$ which is defined with the eigenvalues of seismic structure tensors: $p(\mathbf{x}) = \frac{\lambda_u(\mathbf{x}) - \lambda_v(\mathbf{x})}{\lambda_u(\mathbf{x})}$ (Hale 2009b). As shown in Fig. 12(b), a planarity image ($0 \le p(\mathbf{x}) \le 1$) highlights (with low values) all features that are not planar, such as faults and channels. Therefore, I define the weighting map $q(\mathbf{x}) = 1 - p(\mathbf{x})$ for the semblance equation.

I compute the least-squares solution of the weighted and regularized eq. (30) using the CG method and obtain the structure- and stratigraphy-oriented semblance image shown in Fig. 12(c). With strong smoothness regularization in directions along vectors $\mathbf{w}$, the estimated semblance image (Fig. 12c) displays clear and continuous stratigraphic features such as channels.

In this section, I have applied the method of structure-, stratigraphy-, and fault-guided regularization to real examples of seismic velocity estimation and semblance computation, both of which are formulated as inversion problems. In the first example of velocity estimation, the structure-guided regularization imposes anisotropic and spatially variant smoothness on the velocity model to be inverted. Such anisotropic smoothness is oriented by vectors perpendicular and parallel to layered structures. The strength of smoothness is spatially variant and is defined by the linearity or isotropy of the structures. In areas with linear structures, such smoothness is mainly imposed on the model in directions parallel to structures. In areas with isotropic structures, the smoothness is imposed on the model in all directions and therefore is isotropic. In the first example, fault-guided regularization is also added to the velocity inversion to impose smoothness on the velocity model across faults by following the fault slips that correlate opposite blocks of each fault. With the structure- and fault-guided regularization, the inverted velocity model conforms to both layered structures and faults.

In the second example, I formulate the computation of 3-D seismic semblance as a simple inversion problem, instead of directly computing the semblance ratios. With this formulation, we are able to avoid obtaining wildly varying semblance due to dividing small denominators in computing the semblance ratios. In addition, we can also add structure- and stratigraphy-guided regularization to the inversion formulation of semblance. In this example of detecting seismic channels, I set $\mu_v = 0$ in the regularization because we do not expect to impose smoothness on the semblance in directions laterally perpendicular to the channels, which will blur the channel features in a semblance image. In addition, channels often extend laterally longer along vectors **w** than vertically along vectors **u**. Therefore, I impose stronger smoothness laterally along **w** than vertical along **u** ($\mu_w = 0.9$, $\mu_v = 0.5$) in the regularization to enhance channel features in the semblance image. If we want to compute a semblance image for fault detection, we should impose smoothness in directions along both the fault strike and dip directions to enhance fault features in the semblance image.

## 6 CONCLUSIONS

I have introduced a general scheme to construct convenient structure-, stratigraphy- and fault-guided regularization for geophysical inversion to estimate models that conform to seismic faults, reflectors, and seismic stratigraphic features such as channels.

The regularization requires first estimating structural and stratigraphic orientations and fault slip vectors from a migrated seismic image. The structure- and stratigraphy-guided regularization imposes smoothness on the inverted model along the orientations of structural and stratigraphic features such as seismic reflections and channels. Such regularization is often anisotropic in most areas but can be isotropic in areas where the structural and stratigraphic features are isotropic, which means that the anisotropy or isotropy of the regularization can be spatially variant. The fault-guided regularization, constructed with fault slips, preserves discontinuities at faults and spreads information across faults in the inverted model.

The regularization is especially helpful for inversion with constraints from well-log properties or other geophysical measurements. Such constraints are often limited to only local positions and therefore may have difficulties in providing global control in the inversion. The regularization is helpful to extend the control of the constraints by spreading the properties from the measured positions into the whole inverted model across faults and along structural and stratigraphic orientations.

In all examples discussed in this paper, I assume the properties of the estimated models are consistent with seismic structures and stratigraphic features, which is not necessarily true for some other models. However, we can conveniently vary the regularization for different applications with proper weights ($\mu_u(\mathbf{x})$, $\mu_v(\mathbf{x})$ and $\mu_w(\mathbf{x})$ in eq. 14) to produce desired features in the inverted model. For example, we might want to use different kinds of seismic attributes that highlight reservoirs or discontinuities of subsurface models as weights to construct the regularization.

## ACKNOWLEDGEMENTS

The idea of structure-oriented regularization discussed in this paper is originally from an enlightening talk ‘Structure-oriented Processing and Inversion’ given by Dr Dave Hale in the 2013 sponsor meeting of the Center for Wave Phenomena. I thank Dr Sergey Fomel and Dr Junzhe Sun for inspiring discussions. The seismic image of buried channels is a subset of the Parihaka 3-D data set provided by New Zealand Crown Minerals through the SEG Wiki website (http://wiki.seg.org/wiki/Parihaka-3D). This research is supported by the sponsors of the Texas Consortium for Computational Seismology (TCCS).

## REFERENCES

Ahmed, A.S., Zhou, J., Jardani, A., Revil, A. & Dupont, J., 2015. Image-guided inversion in steady-state hydraulic tomography, *Adv. Water Resour.,* **82,** 83–97.

Arias, E., 2016. Estimating seismic reflection slopes, *Master's thesis,* Colorado School of Mines.

Boschi, L. & Dziewonski, A.M., 1999. High-and low-resolution images of the earth's mantle: implications of different approaches to tomographic modeling, *J. geophys. Res.,* **104**(B11), 25 567–25 594.

Clapp, R.G., Biondi, B.L. & Claerbout, J.F., 2004. Incorporating geologic information into reflection tomography, *Geophysics,* **69**(2), 533–546.

Dix, C.H., 1955. Seismic velocities from surface measurements, *Geophysics,* **20**(1), 68–86.

Engl, H.W., Hanke, M. & Neubauer, A., 1996. *Regularization of Inverse Problems,* Springer Science & Business Media.

Fehmers, G.C. & Höcker, C.F., 2003. Fast structural interpretation with structure-oriented filtering, *Geophysics,* **68**(4), 1286–1293.

Fomel, S., 2002. Applications of plane-wave destruction filters, *Geophysics,* **67**(6), 1946–1960.

Fomel, S., 2007. Shaping regularization in geophysical-estimation problems, *Geophysics,* **72**(2), R29–R36.

Hale, D., 2009a. Image-guided blended neighbor interpolation of scattered data, in *79th Annual International Meeting, SEG, Expanded Abstracts,* pp. 1127–1131.

Hale, D., 2009b. Structure-oriented smoothing and semblance, CWP Report 635.

Hale, D., 2010. Image-guided 3D interpolation of borehole data, in *80th Annual International Meeting, SEG, Expanded Abstracts,* pp. 1266–1270.

Hale, D., 2013a. Dynamic warping of seismic images, *Geophysics,* **78,** S105–S115.

Hale, D., 2013b. Methods to compute fault images, extract fault surfaces, and estimate fault throws from 3D seismic images, *Geophysics,* **78**(2), O33–O43.

Hale, D., 2013c. Structure-oriented processing and inversion, in *2013 Project Review meeting of the Consortium Project on Seismic Inverse Methods for Complex Structures*, Colorado School of Mines, Golden, US.

Inoue, H., Fukao, Y., Tanabe, K. & Ogata, Y., 1990. Whole mantle *P*-wave travel time tomography, *Phys. Earth planet. Inter.*, **59**(4), 294–328.

Jackson, D.D., 1972. Interpretation of inaccurate, insufficient and inconsistent data, *Geophys. J. Int.,* **28**(2), 97–109.

Li, Y. & Oldenburg, D.W., 2000. Incorporating geological dip information into geophysical inversions, *Geophysics,* **65**(1), 148–157.

Ma, Y., Hale, D., Gong, B. & Meng, Z.J., 2012. Image-guided sparse-model full waveform inversion, *Geophysics,* **77**(4), R189–R198.

Marfurt, K.J., Kirlin, R.L., Farmer, S.L. & Bahorich, M.S., 1998. 3-D seismic attributes using a semblance-based coherency algorithm, *Geophysics,* **63**(4), 1150–1165.

Marfurt, K.J., Sudhaker, V., Gersztenkorn, A., Crawford, K.D. & Nissen, S.E., 1999. Coherency calculations in the presence of structural dip, *Geophysics,* **64**(1), 104–111.

Revil, A. & Cathles, L., 2002. Fluid transport by solitary waves along growing faults: a field example from the South Eugene Island Basin, Gulf of Mexico, *Earth planet. Sci. Lett.,* **202**(2), 321–335.

Russell, B., Hampson, D. & Bankhead, B., 2006. An inversion primer, *CSEG Recorder,* **31,** 96–102.

Tikhonov, A., 1963. Solution of incorrectly formulated problems and the regularization method, *Sov. Math. Dokl.,* **5,** 1035–1038.

Trampert, J. & Woodhouse, J.H., 1995. Global phase velocity maps of Love and Rayleigh waves between 40 and 150 seconds, *Geophys. J. Int.,* **122**(2), 675–690.

Valenciano, A.A., Brown, M. & Guitton, A., 2004. Interval velocity estimation using edge-preserving regularization, in *74th Annual International Meeting, SEG, Expanded Abstracts,* pp. 2431–2434.

Van Vliet, L.J. & Verbeek, P.W., 1995. Estimators for orientation and anisotropy in digitized images, in *Proceedings of the first annual conference of the Advanced School for Computing and Imaging ASCI'95,* Heijen, The Netherlands, pp. 442–450.

VanDecar, J.C. & Snieder, R., 1994. Obtaining smooth solutions to large, linear, inverse problems, *Geophysics,* **59**(5), 818–829.

Weickert, J., 1997. A review of nonlinear diffusion filtering, in *Scale-Space Theory in Computer Vision,* vol. 1252 of Lecture Notes in Computer Science, pp. 1–28, eds ter Haar Romeny, B., Florack, L., Koenderink, J. & Viergever, M., Springer.

Wu, X., 2017. Directional structure-tensor based coherence to detect seismic faults and channels, *Geophysics,* **82**(2), A13–A17.

Wu, X. & Hale, D., 2015. Horizon volumes with interpreted constraints, *Geophysics,* **80,** IM21–IM33.

Wu, X. & Hale, D., 2016. 3D seismic image processing for faults, *Geophysics,* **81**(2), IM1–IM11.

Wu, X., Luo, S. & Hale, D., 2016. Moving faults while unfaulting 3D seismic images, *Geophysics,* **81**(2), IM25–IM33.

Zhang, J. & Revil, A., 2015. 2d joint inversion of geophysical data using petrophysical clustering and facies deformation, *Geophysics,* **80**(5), M69–M88.

Zhang, X. & Zhang, J., 2012. Edge preserving regularization for seismic traveltime tomography, in *82nd Annual International Meeting, SEG, Expanded Abstracts,* pp. 1–5.

Zhdanov, M., 2002. *Geophysical Inverse Theory and Regularization Problems,* Elsevier Science.

Zhou, J., Revil, A., Karaoulis, M., Hale, D., Doetsch, J. & Cuttler, S., 2014. Image-guided inversion of electrical resistivity data, *Geophys. J. Int.,* **197,** 292–309.

Zhou, J., Revil, A. & Jardani, A., 2016. Stochastic structure-constrained image-guided inversion of geophysical data, *Geophysics,* **81**(2), E89–E101.